# Zero offset seismic resolution theory for linear v(z)

Gary F. Margrave


## SUMMARY

From the perspective of f-$k_x$ migration theory, the optimizing the ability of seismic data to resolve earth features requires maximization of the spectral bandwidth after migration. The $k_x$ (horizontal wavenumber) bandwidth determines the lateral resolution and is directly proportional to the maximum frequency and the sine of the maximum scattering angle and inversely proportional to velocity. Constraints on the maximum scattering angle can be derived by examining the three effects of finite spatial aperture, finite recording time, and discrete spatial sampling. These effects are analyzed, assuming zero-offset recording, for the case of a linear (constant gradient) v(z) medium. Explicit analytic expressions are derived for the limits imposed on scattering angle for each of the three effects. Plotting these scattering angle limits versus depth limits for assumed recording parameters is an effective way to appreciate their impact on recording. When considered in context with f-k migration theory, these scattering angle limits can be seen to limit spatial resolution and the possibility of recording specific reflector dips. Seismic surveys designed with the linear v(z) theory are often much less expensive than constant velocity theory designs.


## INTRODUCTION

Seismic line length and maximum record time place definite limits on the maximum scattering angle that can be recorded, and hence imaged, on a migrated zero offset section. Since horizontal resolution depends directly on the sine of the maximum scattering angle (Vermeer, 1990 and many others), it is important to understand these effects for survey design and interpretation. Furthermore, the observation of a normal incidence reflection from a dipping reflector requires having a scattering angle spectrum whose limits exceed the reflector dip.

The imposition of finite recording apertures in space and time actually imprints a strong spatial-temporal variation (i.e. nonstationarity) on the spectral content of a migrated section. As an example, consider the synthetic seismic section shown in Figure 1a. This shows a zero offset (constant velocity) simulation of the response of a grid of point scatterers (diffractors) distributed uniformly throughout the section. Note how the diffraction responses change geometry and how the recording apertures truncate each one differently. Figure 1b is a display of the f- $k_x$ amplitude spectrum for this section. As expected from elementary theory, all energy is confined to a triangular region defined by $|k_x|<f/v$ ($k_x$ is horizontal wavenumber, f is temporal frequency, and v is velocity).

Figure 2a shows this section after a constant velocity f-k migration and Figure 2b is the f- $k_x$ spectrum after migration. The spectrum shows the expected behavior in that the triangular region of Figure 1b has unfolded into a circle. Essentially, each frequency (horizontal line in Figure 1b) maps to a circle in Figure 2b (see Chun and Jacewitz, 1981 for a discussion). Note that f-k migration theory as usually stated (Stolt, 1978) assumes infinite apertures while close inspection of the focal points in Figure 2a shows that their geometry varies strongly with position.

The four focal points shown boxed in Figure 2a are enlarged in Figure 3a. Considering the focal points near the center of the spatial aperture, a small, tight focal

point at the top of the section grades to a broad, dispersed smear near the bottom. Alternatively, assessing at constant time shows the focal points grading from strongly asymmetric-left through symmetric to asymmetric-right. Figure 3b shows local f- $k_x$ spectra of the four focal points in Figure 3a. Comparing with Figure 2b shows that these local spectra are dramatically different from the global spectrum. Only the top-center point has the full circular spectrum expected from the infinite aperture theory while the others show strong asymmetry or severe bandwidth restrictions. These local spectra determine the local resolution characteristics of the aperture limited seismic section. Schuster (1997) gives a formal theory (assuming constant velocity) for these focal points and shows that the local spectra are bounded by scattered rays that extend from the scatter point to either side of the section. This current paper shows how to estimate these scattering angles in a realistic setting and therefore how to assess resolution implications.

For constant velocity, the computation of limiting scattering angles is well understood but this approach often results in overly expensive survey designs. An analysis with a constant velocity gradient is much more realistic as it allows for first order effects of ray bending by refraction. Such an analysis is presented here together with a simple graphical method of assessing the results.

## THEORY

Stolt (1978) established f-k migration theory for the post-stack, zero-offset case. A fundamental result is that constant velocity migration is accomplished by a mapping from the $(k_x,\omega)$ plane to the $(k_x,k_z)$ plane as illustrated in Figure 4. As can be deduced from the figure, the $k_x$ bandwidth after migration is limited by:

$$k_{x\,lim} = k_{x\,max}\sin\left(\theta_{max}\right) = \frac{2f_{max}\sin\left(\theta_{max}\right)}{v} \quad . \tag{1}$$

In this expression, $k_{xmax}$ is the limiting wavenumber to be expected from a migration with no limitation on scattering angle. In any practical setting, there is always a limit on scattering angle and it is generally spatially variant. The limit may be a result of the effects of finite aperture, finite record length, and discrete spatial sample size or any of many other possibilities including: the migration algorithm may be “dip limited”, lateral or complex vertical velocity variations can create shadow zones, attenuation effects are dependent on raypath length and hence affect the larger scattering angles more. Whatever, the cause, a limitation of the range of scattering angles which can be collected and focused to a particular point translates directly into a resolution limit as expressed by equation (1). The size of the smallest resolvable feature, say $\delta x$, is inversely proportional to $k_{xlim}$. For definiteness, let $k_{xlim} = \alpha/(2\delta x)$, where $\alpha$ is a proportionality constant near unity, and solve for $\delta x$ to get:

$$\delta x = \frac{\alpha\, v}{4f_{max}\sin\left(\theta_{max}\right)} \quad . \tag{2}$$

Since the aperture limit is x and z variant (and record length and spatial aliasing limits are z variant) $\delta x$ must also vary with position. An interpretation of equation (2) is that it gives the smallest discernible feature on a reflector whose dip is normal to the bisector of the scattering angle cone at any position (Figure 5).

For constant velocity, the limits imposed on zero-offset scattering angle are easily derived using straight ray theory and have been shown (Lynn and Deregowski, 1981) to be:

$$\tan\left(\theta_A\right) = \frac{A}{z} \quad , \tag{3}$$

$$\cos\left(\theta_T\right) = \frac{vT}{2z} \quad . \tag{4}$$

In these expressions, A is the available aperture, T is the record length, z is depth, and v is the presumed constant velocity. $\theta_A$ and $\theta_T$ are limitations on scattering angle imposed by aperture and record length respectively (Figure 5). Aperture is defined as the horizontal distance from an analysis point to the end of the seismic line or the edge of a 3-D patch and is thus dependent on azimuth and position (Figure 6). Alternatively, the record length limit has no lateral variation. Taken together, these expressions limit the scattering angle spectrum to a recordable subset.

A third limiting factor is spatial aliasing which further constrains the possible scattering angle spectrum to that which can be properly imaged (migrated). (Liner and Gobeli, 1996 and 1997, give an analysis of spatial aliasing in this context.) The Nyquist requirement is that there must be at least two samples per horizontal wavelength to avoid aliasing:

$$\lambda_x \geq 2\Delta x \text{ where } \lambda_x = \frac{\lambda}{\sin\left(\theta_x\right)} \quad . \tag{5}$$

Here, $\Delta x$ is the spatial sample size (cdp interval), $\lambda$ and $\lambda_x$ are wavelength and its apparent horizontal component, and $\theta_x$ is most properly interpreted as the emergence angle of a dipping event on a zero offset section. Consistent with zero offset migration theory, the exploding reflector model (Lowenthal et al., 1976) can be used to relate wavelength to velocity through $\lambda = v/(2f)$ where f is some frequency of interest. This leads to an angle limited by spatial aliasing given by:

$$\sin\left(\theta_x\right) = \frac{v}{4f\Delta x} \quad . \tag{6}$$

In the constant velocity case, the emergence angle of a ray and the scattering angle at depth are equal and thus equation (6) expresses the constant velocity limit on scattering angle imposed by spatial aliasing. For vertical velocity variation, v(z), the result still applies provided that $\theta_x$ is simply interpreted as emergence angle and v as near surface velocity. The emergence angle can be related to the scattering angle at depth using Snell's law. This is done by recalling that the ray parameter, $p = \sin(\theta(z))/v(z)$, is conserved (Slotnick, 1959), which leads to

$$\sin\left(\theta_x\right) = \frac{v(z)}{4f\Delta x} \quad . \tag{7}$$

This expression generalizes spatial aliasing considerations to monotonically increasing but otherwise arbitrary v(z) and $\theta_x$ is interpreted as the scattering angle from depth, z.

Returning to constant velocity, equations (3), (4), and (6) can be used to create a scattering angle resolution chart for an assumed recording geometry, position on the line, frequency of interest and constant velocity. A typical case is shown in Figure 7 where it is seen that the aperture limit is concave upward and tends asymptotically to zero at infinite depth. The record length limit has the opposite curvature and reaches zero degrees at the depth z = vT/2. Both limits admit the possibility of 90° only for z=0. The spatial aliasing limit is depth independent but requires a frequency of interest which can conservatively be taken as the maximum (not dominant) signal frequency.

Charts such as Figure 7 can be used as an aid in survey design but tend to give unrealistic parameter estimates due to the assumption of straight raypaths. In most exploration settings, velocity increases systematically with depth and thus raypaths bend upward as they propagate from the scatterpoint to the surface. Intuitively, this should lead to shorter aperture requirements and allow the possibility of recording scattering angles beyond 90° in the near surface. The spatial aliasing limit has already been discussed in this context and the aperture and record length limits will now be derived exactly for the case of a constant velocity gradient, that is when $v(z) = v_o + cz$. The derivation requires solution of the Snell's law raypath integrals for the linear gradient case (Slotnick 1959). If $p_A$ is the ray parameter required to trace a ray from a scatterpoint to the end of the spatial aperture, then

$$A(z) = \int_0^z \frac{p_A v(z)}{\sqrt{1 - p_A^2 v(z)^2}} dz \quad . \tag{8}$$

Similarly, let $p_T$ be the ray parameter for that ray from scatterpoint to the surface which has traveltime (two-way) equal to the seismic record length, then

$$T(z) = \int_0^z \frac{1}{v(z)\sqrt{1 - p_T^2 v(z)^2}} dz \quad . \tag{9}$$

These integrals can be computed exactly, letting $v(z) = v_o + cz$, to give

$$A = \frac{1}{p_A c}\left( \sqrt{1 - p_A^2 v_0^2} - \sqrt{1 - p_A^2 v(z)^2} \right) \quad , \tag{10}$$

and

$$T = \frac{2}{c} \ln \left[ \frac{v(z)}{v_0} \left( \frac{1 + \sqrt{1 - p_T^2 v_0^2}}{1 + \sqrt{1 - p_T^2 v(z)^2}} \right) \right] \quad . \tag{11}$$

Equations (10) and (11) give spatial aperture, A, and seismic record length, T, as a function of ray parameter and velocity structure.

Letting $p_A = \sin(\theta_A(z))/v(z)$ and $p_T = \sin(\theta_T(z))/v(z)$, equations (10) and (11) can both be solved for scattering angle to give

$$\sin^2\left(\theta_A\right) = \frac{\left(2Acv_0\gamma\right)^2}{\left(A^2c^2 + v_0^2\right)^2\gamma^4 + 2v_0^2\gamma^2\left(A^2c^2 - v_0^2\right) + v_0^4} \quad , \tag{12}$$

and

$$\cos\left(\theta_T\right) = \frac{\gamma^{-1} - \cosh\left(cT/2\right)}{\sinh\left(cT/2\right)} \quad , \tag{13}$$

where $$\gamma = \frac{v_0}{v(z)} \quad .$$

When equations (9), (11), and (12) are used to create a scattering angle resolution chart, the result is typified by Figure 8. The parameters chosen are the same as for Figure 6 and the linear velocity function was designed such that it reaches 3500 m/s (the value used in Figure 7) in the middle of the depth range of Figure 7. It can be seen that the possibility of recording angles beyond 90° is predicted for the first 1000 m and the aperture limit is everywhere more broad than in Figure 7. The record length limit forces the scattering angle spectrum to zero at about 3700 m compared to over 5000 m in the constant velocity case. This more severe limit is not always the case, in fact a record length of 6 seconds will penetrate to over 12000 m in the linear velocity case and only 10500 m in the constant case. Also apparent is the fact that the spatial aliasing limit predicts quite severe aliasing in the shallow section though it gives exactly the same result at the depth where v(z) = 3500 m/s.

## EXAMPLES

Figures 9, 10, and 11 provide further comparisons between the linear v(z) theory and constant velocity results. In Figure 9, the aperture limits are contrasted for the same linear velocity function (v = 1500 +.6 z m/s) and constant velocity (v 3500 m/s) used before. The dark curves show the linear velocity results and the light curves emanating from 90° at zero depth are the constant velocity results. Each set of curves covers the range of aperture values (from top to bottom): 1000, 4000, 12000, and 20000 meters. The dramatic effect of the v(z) theory is especially obvious for larger apertures which admit angles beyond 90° for a considerable range of depths. Figure 10 is similar to Figure 9 except that the record length limit is explored. For each set of curves, the record lengths shown are (from top to bottom): 2.0, 4.0, 6.0, and 8.0 seconds. Figure 11 shows spatial aliasing limits for a frequency of 60 Hz and a range of $\Delta x$ values (from top to bottom): 10 20 40 60 80 100 and 150 meters.

Next consider Figure 12 which shows a synthetic demonstration of the *aperture effect*. Here, a number of unaliased point diffractor responses have been arranged at constant time. Thus the record length limit is constant and the aliasing limit does not apply. When migrated, the resulting display clearly shows the effect of finite spatial aperture on resolution. Comparison with Figure 6 shows the direct link between recorded scattering angle spectrum and resolution. Approximately, the focal points appear as dipping reflector segments oriented such that the normal (to the segment) bisects the captured scattering angle spectrum.

Figure 13 is a study designed to isolate the effects of temporal record length on resolution. The unmigrated section is constructed such that all five point diffractors are limited by record length and not by any other effect. Upon migration, the focal points

are all symmetric about a vertical axis but show systematic loss of lateral resolution with increasing time. As shown in Figures 7, 8, and 10, the record length limit always forces the scattering angle spectrum to zero at the bottom of the seismic section. Equation 2 then results in a lateral resolution size that approaches infinity. This effect accounts for the often seen data 'smearing' at the very bottom of seismic sections.

Figure 14 shows the migration of a single diffraction hyperbola with three different spatial sample intervals to illustrate the resolution degradation that accompanies spatial aliasing. In Figure 14B, the migration was performed with a spatial sample rate of 4.5 m which represents a comfortably unaliased situation. In Figures 14C and 14D the sample intervals are 9 m (slightly aliased) and 18 m (badly aliased). The slightly aliased situation has not overly compromised resolution but the badly aliased image is highly degraded. Note that the vertical size of the image is unaffected.

In Figure 15, the effect of maximum temporal frequency is examined. A single diffraction hyperbola was migrated with three different maximum frequency limits . In Figure 15B, the focal point and its local f-$k_x$ spectrum are shown for an 80 Hz maximum frequency while Figures 15C and 15D are similar except that the maximum frequency was 60 Hz and 40 Hz respectively. It is clear from these figures that limiting temporal frequency affects both vertical and lateral resolution. As expected from equation (2), a reduction of $f_{max}$ from 80 Hz to 40 Hz causes a doubling of the focal point size.

Finally Figure 16 is a simple resolution simulation using equation (2) with the constant a set to unity and the scattering angle spectrum computed using the constant velocity limiting equations (3) and (4). Comparison of 16A) with Figure 2A) and 16B) with Figure 3A) shows a reasonable, if simplistic, agreement. This merely shows that the simple resolution concepts given here go a long way towards explaining the spatial variation of resolution beneath a seismic survey. In a practical setting, it is recommended that actual wave equation diffraction synthetics be generated and migrated or that the constant velocity migration Green's function of Schuster (1997) be used.

## CONCLUSIONS

The theory of f-$k_x$ migration predicts a simple model for the resolving power of seismic data. The result is a spatial bandwidth that depends directly on frequency and sine of scattering angle and inversely on velocity. Finite recording parameters (aperture and record length) place space and time variant limits on the observable scattering angle spectrum. Thus the resolution of a seismic line is a function of position within the aperture of the line. The scattering angle limits imposed by aperture, record length, and spatial sampling can be derived exactly for the case of constant velocity and for velocity linear with depth. The linear velocity results are more realistic and lead to considerably different, and usually cheaper, survey parameters than the constant velocity formulae.

## ACKNOWLEDGMENTS

I originally developed this theory in 1983 while I was employed by Chevron Corporation. I am grateful to Chevron for allowing me to publish it and I thank the sponsors of the CREWES Project for their support.

## REFERENCES

Chun, J. H., and Jacewitz, C. A., 1981, Fundamentals of frequency domain migration: Geophysics, **46**, 717-733.

Lowenthal, D., Lou, L., Robertson, R., and Sherwood, J. W., 1976, The wave equation applied to migration, Geophys. Prospect., 24, 380-399.

Liner, C. T., 1996, Bin size and linear v(z): Expanded abstracts, 66th Annual Mtg. Soc. Expl. Geophy., 47-50.

Liner, C. T., 1997, 3-D seismic survey design and linear v(z): Expanded abstracts, 67th Annual Mtg. Soc. Expl. Geophy., 47-50.

Lynn, H. B. and Deregowski, S., 1981, Dip limitations on migrated sections as a function of line length and recording time, Geophysics, 46, 1392-1397.

Schuster, G. T., 1997, Green's function for migration: Expanded Abstracts, 67th Annual Mtg. Soc. Expl. Geophy., 1754-1757

Stolt, R. H., 1978, Migration by Fourier transform: Geophysics, **43**, 23-48.

Slotnick, M. M., 1959, Lessons in Seismic Computing, Society of Exploration Geophysicists.

Vermeer, G, 1990, Seismic wavefield sampling Society of Exploration Geophysicists.

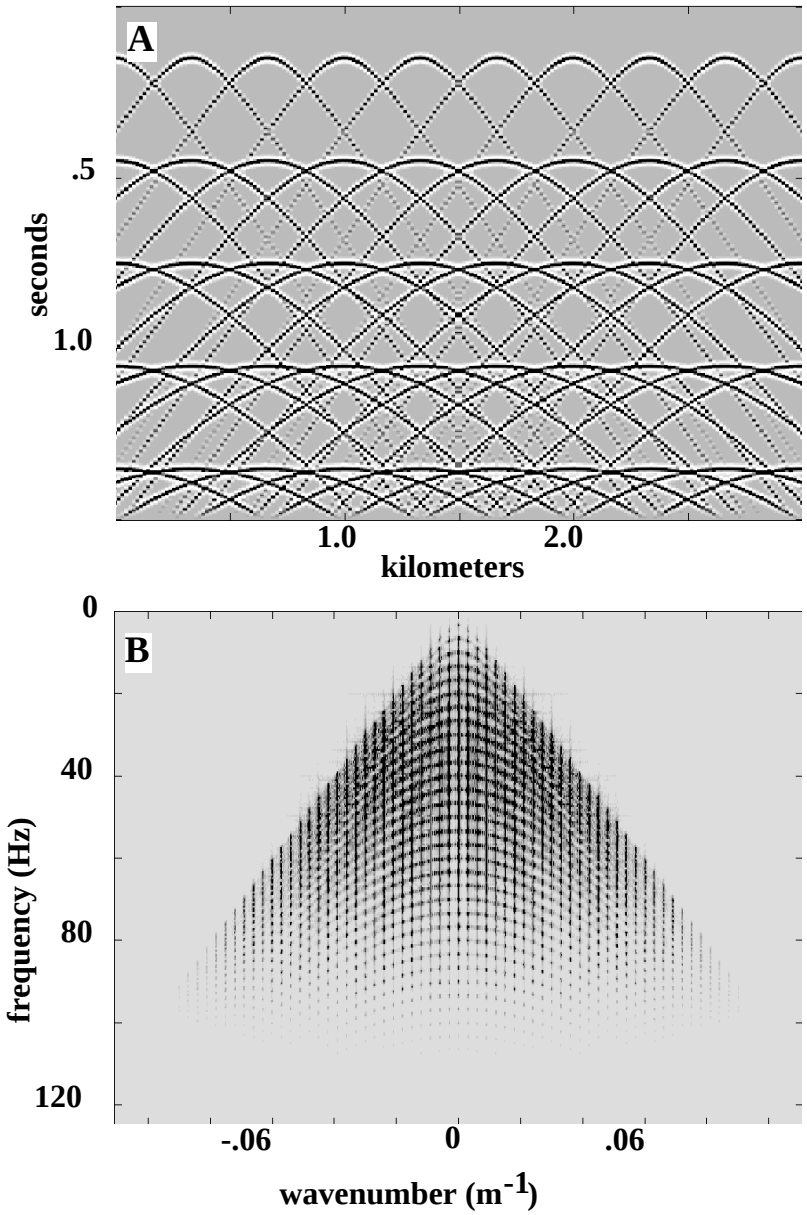


Fig. 1. A) A constant velocity synthetic seismic section constructed from a grid of point scatterers assuming zero offset recording geometry. B) f-$k_x$ spectrum of the section in A.

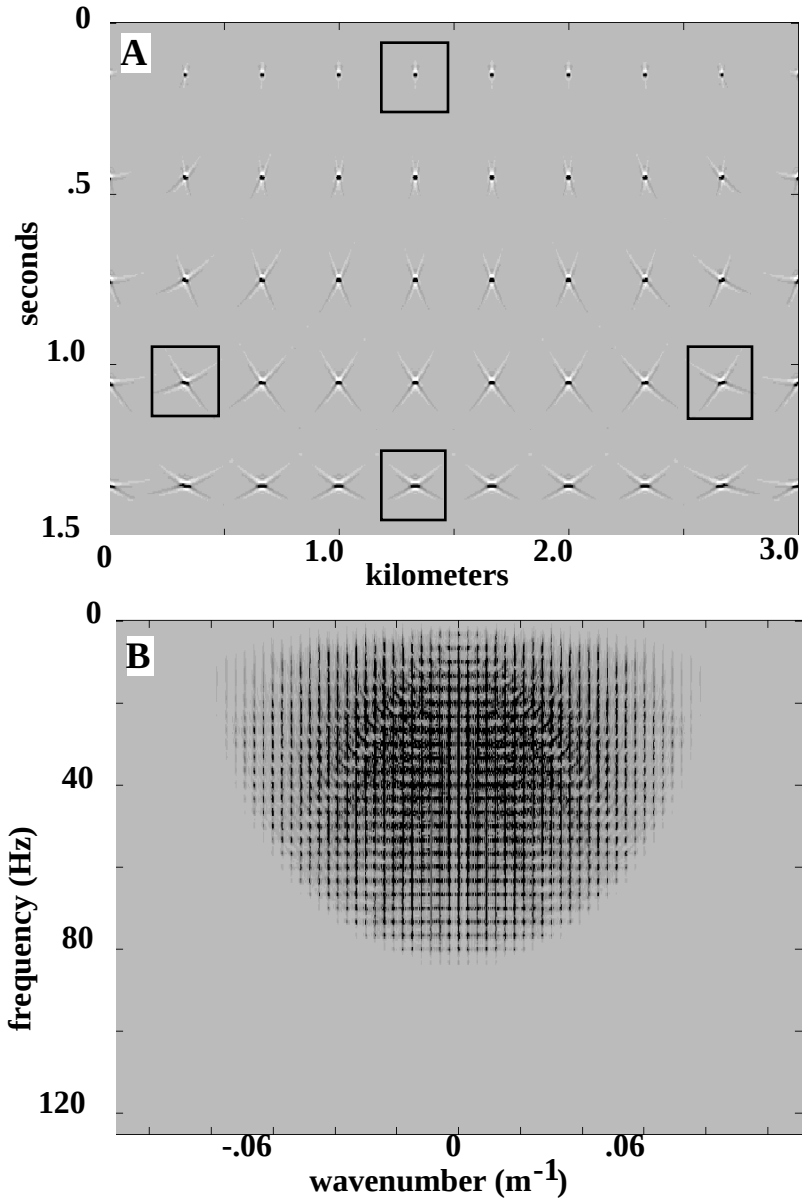


Fig. 2. A) Result from f-$k_x$ migration of the synthetic section in Figure 1A. Boxes denote locations of zoomed images in Figure 3. B). f-$k_x$ spectrum of the section in A.

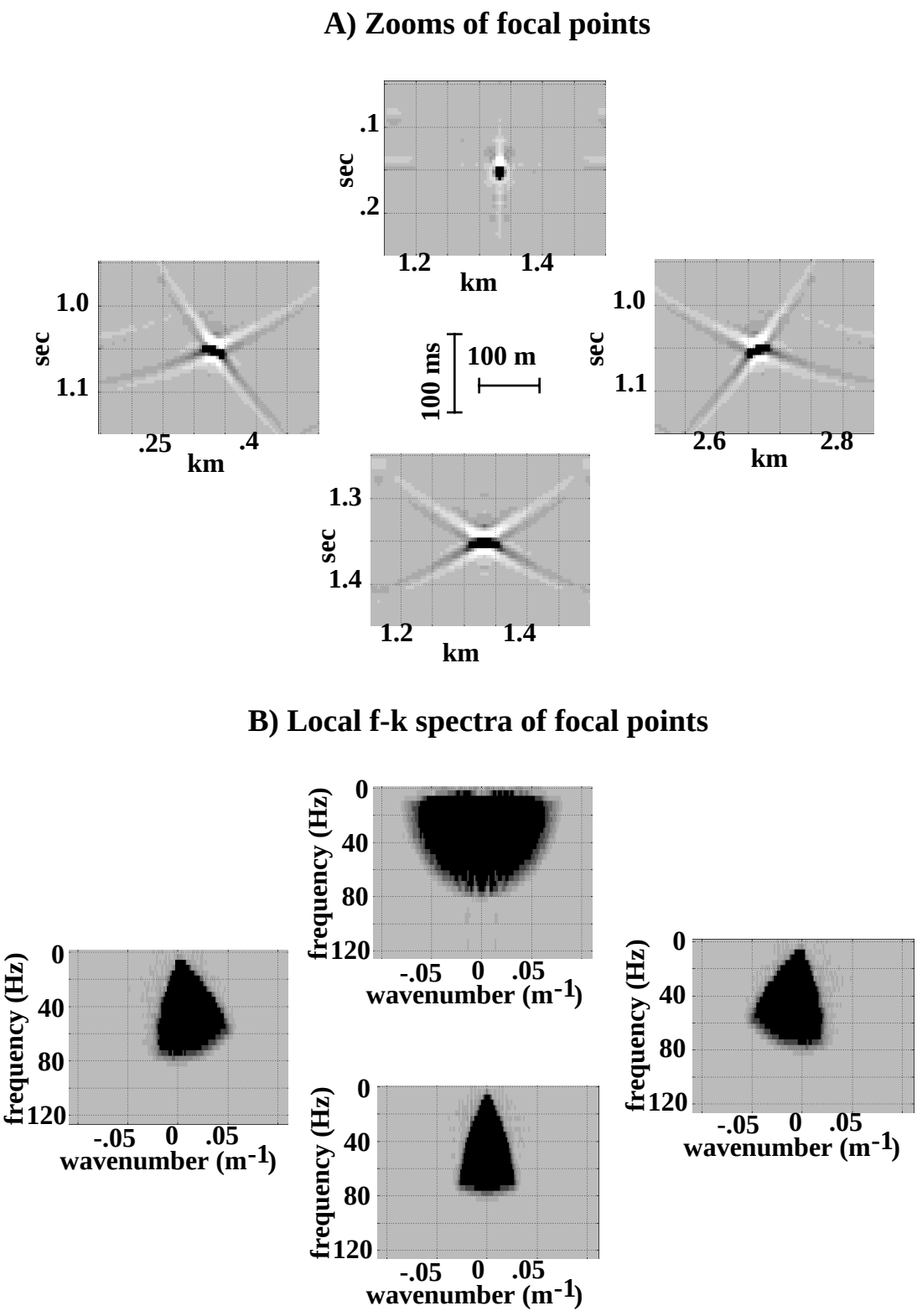


Fig. 3. A) Zooms of the four focal points indicated by boxes in Figure 2A. B) f-$k_x$ spectra of the four images in A.

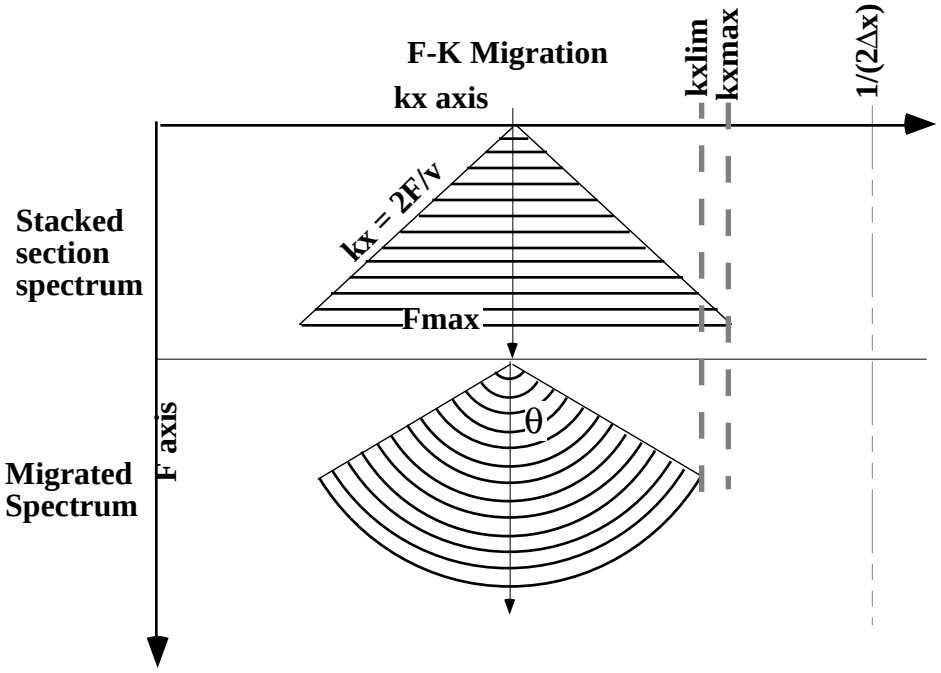


Fig. 4. Constant velocity f-k migration theory relates the f-k spectra before and after migration through a vertical mapping and an angle limitation.

**Zero offset scattering**

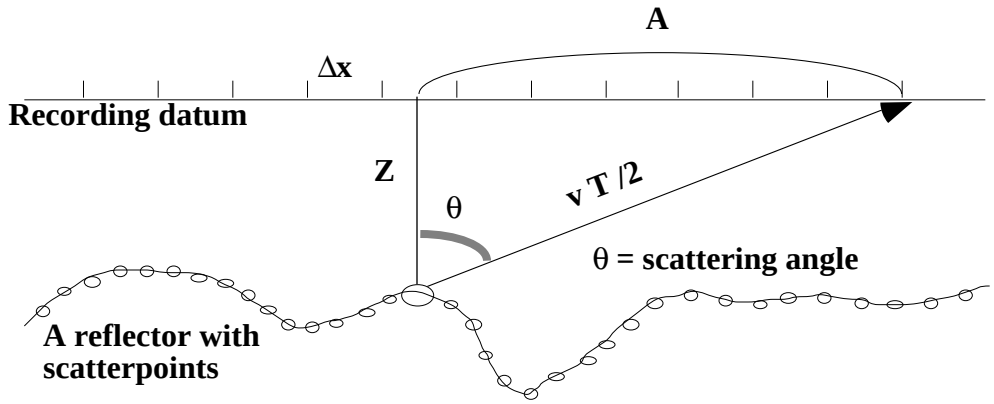


Fig. 5: Recording aperture, A, record length, V, and spatial sampling interval Δx all limit the scattering angle spectrum after migration.

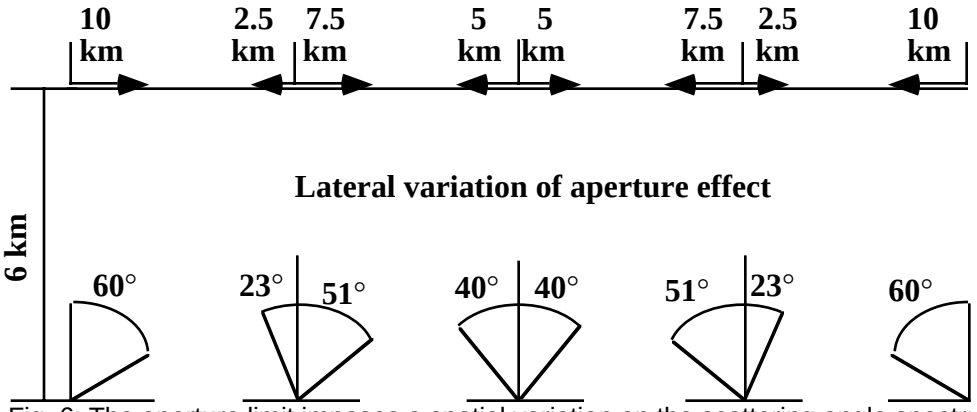


Fig. 6: The aperture limit imposes a spatial variation on the scattering angle spectrum.

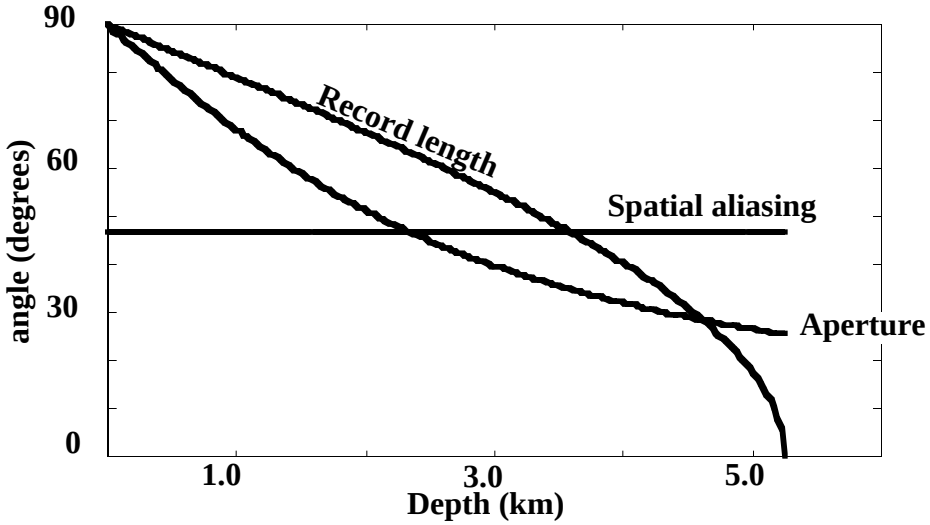


Fig. 7: Constant velocity scattering angle chart showing: aperture limit, record length limit and spatial aliasing limit for a case when A=2500 m, T=3.0 sec, v=3500 m/s, $\Delta x$ = 20 m, and f=60.

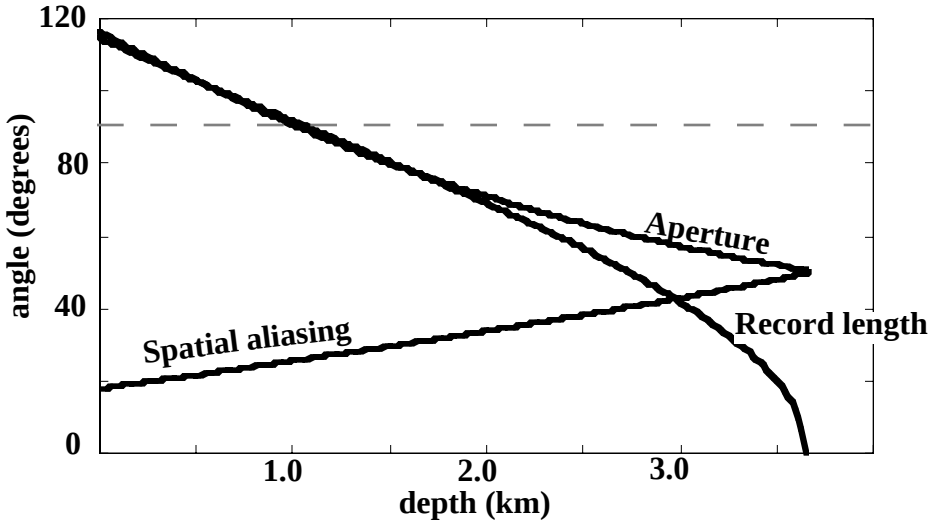


Fig. 8: Constant gradient scattering angle chart showing: aperture limit, record length limit, and spatial aliasing limit for a case when A=2500 m, T=3.0 sec, v = 1500 + .6z m/s, $\Delta x$ = 20 m, and f=60.

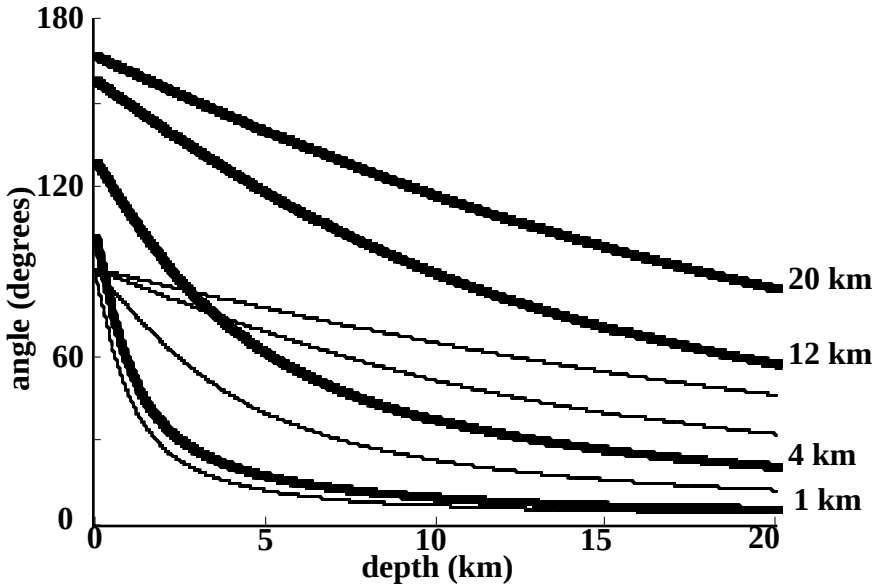


Fig. 9. Aperture limit curves for the linear velocity function, v = 1500 +.6 z m/s, (bold) and the constant velocity of 3500 m/s. Each set of curves shows the apertures (from top to bottom): 1000, 4000, 12000, and 20000 meters.

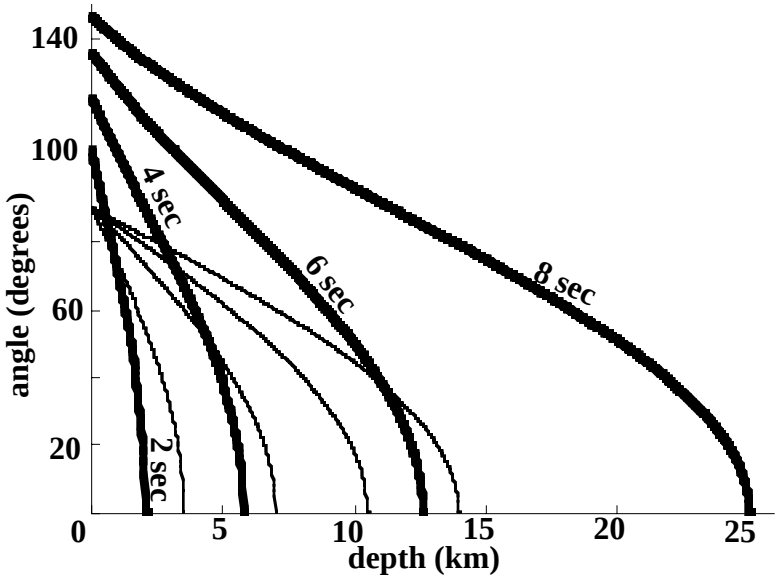


Fig. 10. Record limit curves for the case of Figure 6. Record lengths shown (top to bottom): 2.0, 4.0, 6.0, and 8.0 seconds.

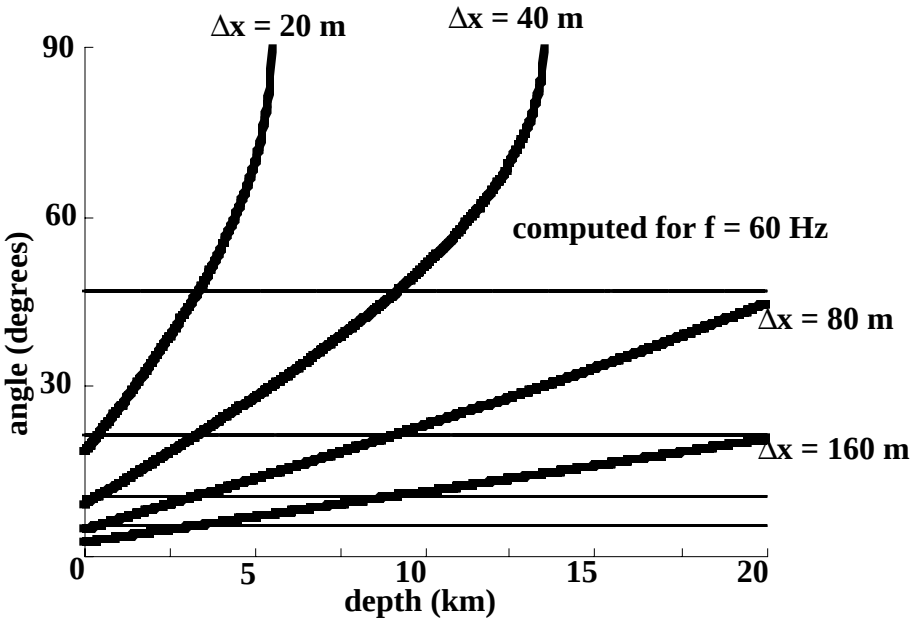


Fig. 11. Spatial aliasing limit curves (assuming 60 Hz) for the same case as Figure 6. Spatial sample rates (top-left to bottom-right): 10 20 40 60 80 100 and 150 meters.

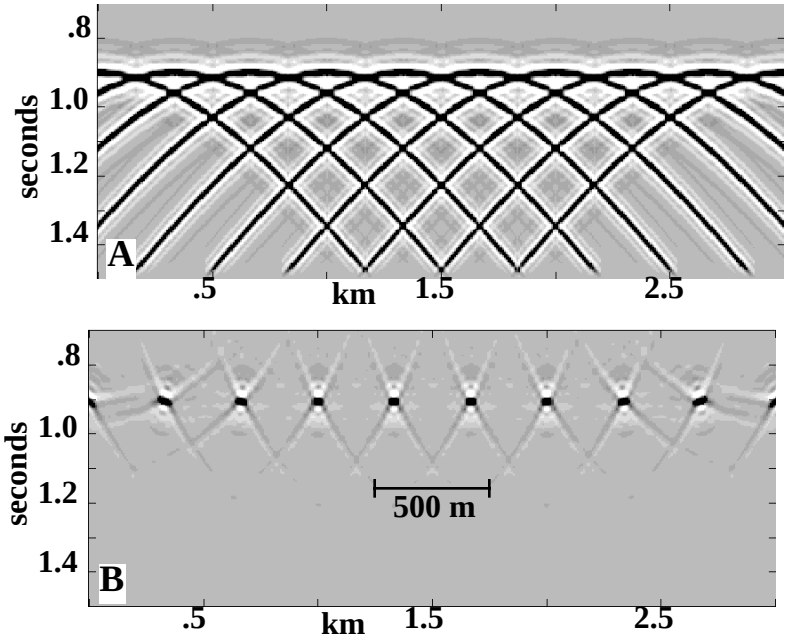


Fig. 12. An illustration of the aperture effect. All of the synthetic diffractions in A have an identical record length limit and have no spatial aliasing. Thus, only the aperture limit on scattering angle varies with each diffractor. The migrated result is shown in B. Compare with Figure 6.

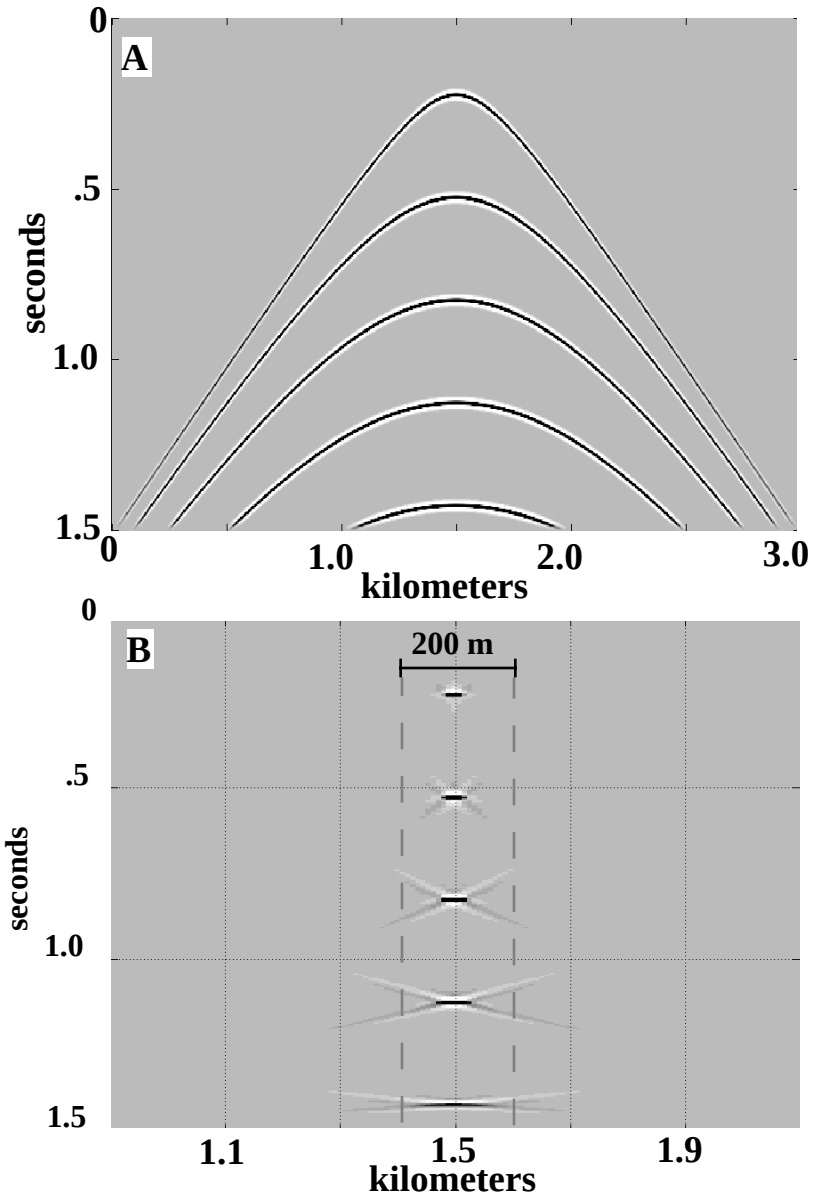


Fig. 13. An illustration of the record length effect. The diffractions in A) are limited only by the record length. The migrated result in B) shows a systematic loss of lateral resolution with increasing time. At the bottom of the section, the lateral size of the focal point is theoretically infinite. Note the horizontal scale change between A) and B).

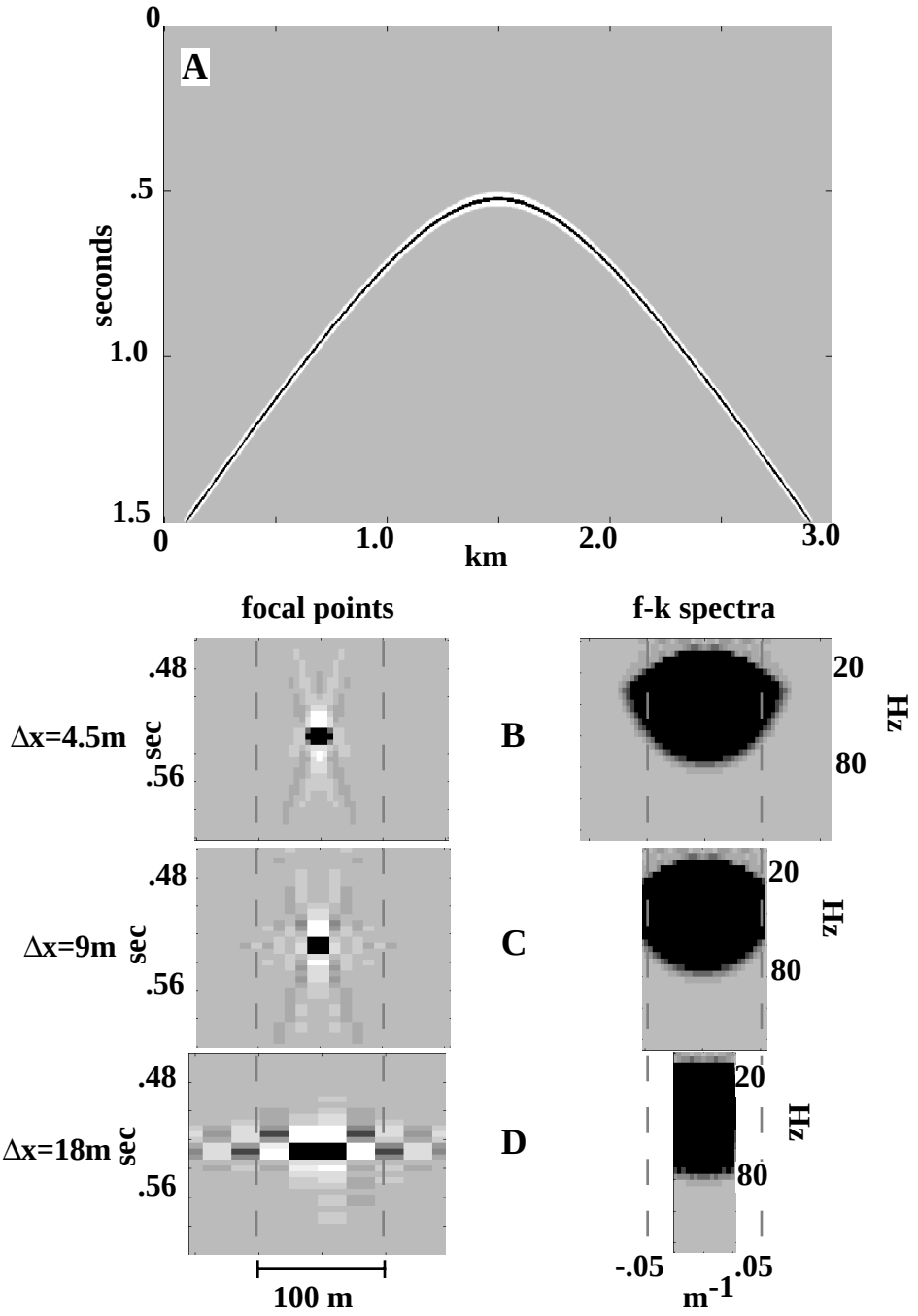


Fig. 14. An illustration of the spatial aliasing effect. A) shows a single diffraction hyperbola. B) shows a zoom of the focal point and the f-$k_x$ spectrum after a migration with a spatial sample rate of 4.5m. C) and D) are similar results after migrations with spatial sample rates of 9m and 18m respectively.

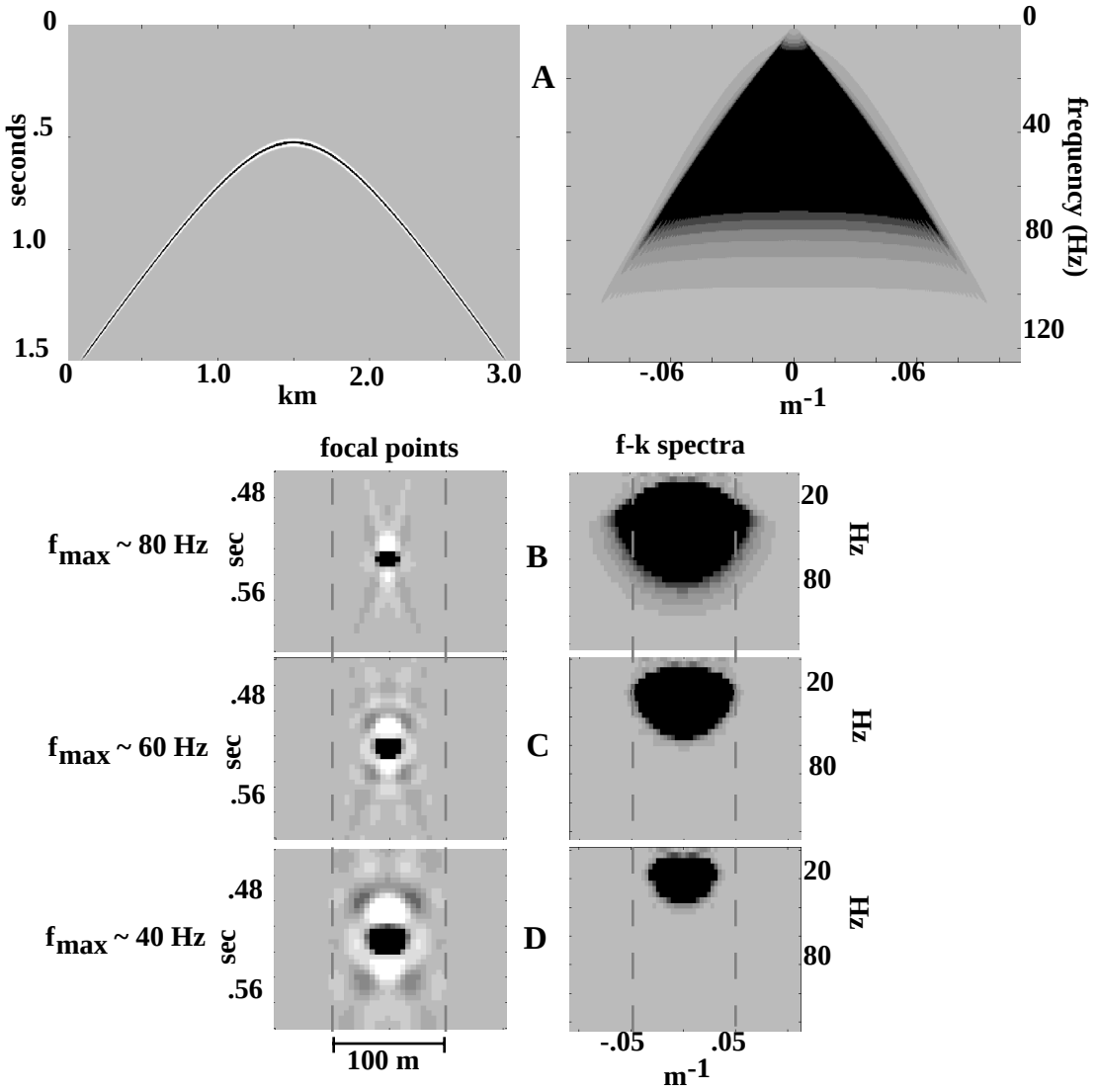


Fig. 15. An illustration of the effect of maximum frequency on resolution. A) A single diffraction hyperbola and its f-$k_x$ spectrum. B) The focal point and its f-$k_x$ spectrum after migration with a maximum frequency of 80Hz. C) and D) are similar to B) except that the maximum frequency was 60Hz and 40Hz respectively.

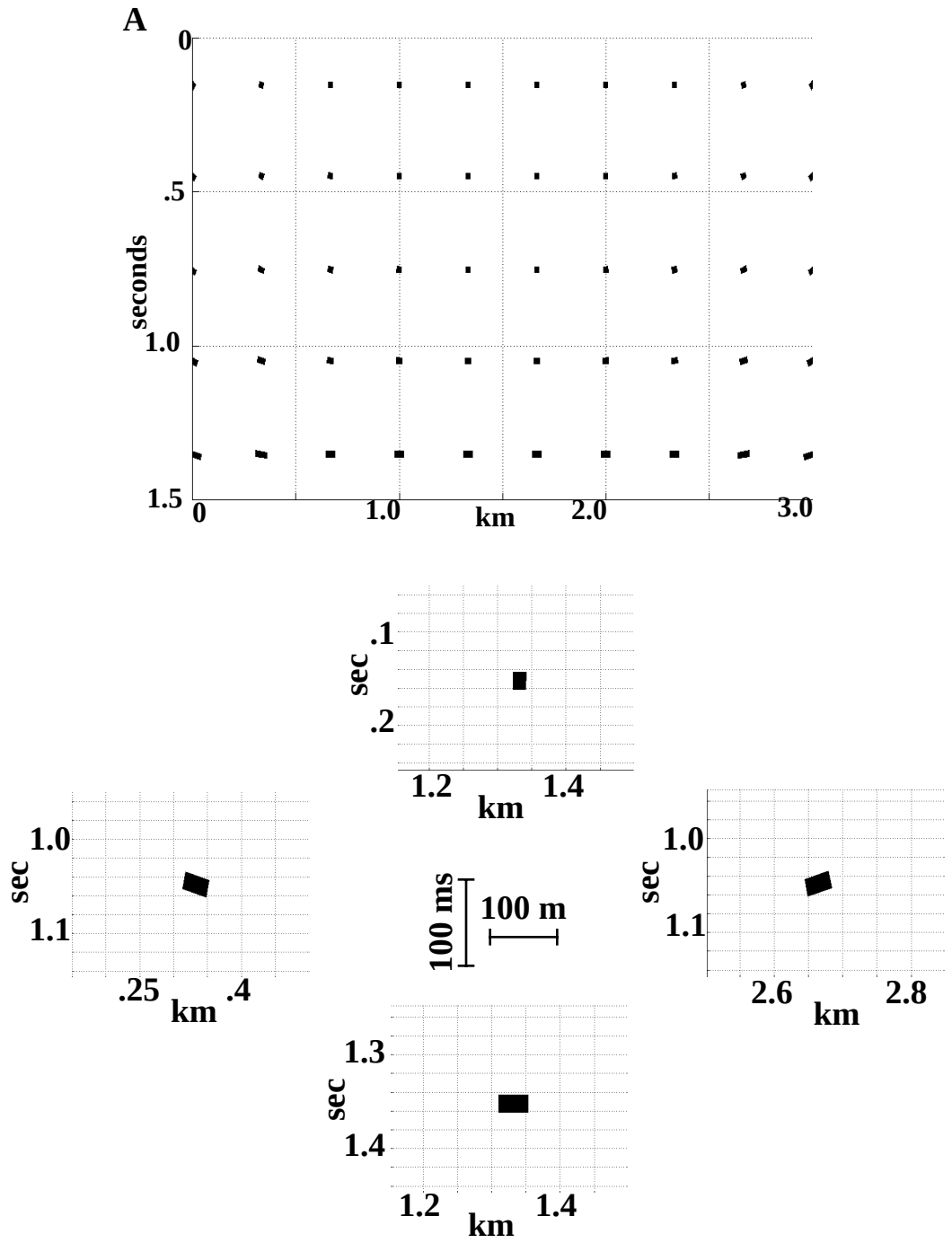


Fig. 16. Synthetic resolution simulation using equation (2) and limiting the scattering angle spectrum according to the effects described in the paper. Compare A) with Figure 2A) and B) with Figure 3A).